PAPER

Probing the effect of the Si/Al ratio in Cu-CHA zeolite catalysts on SO$_2$ exposure: *in situ* DR UV-vis spectroscopy and deactivation measurements†

Reza K. Abasabadi, [ID] [ab] Ton V. W. Janssens, [ID] *[a]
Silvia Bordiga [ID] [b] and Gloria Berlier [ID] *[b]

Cu-exchanged chabazite zeolite (Cu-HA) is one of the most effective catalysts for ammonia-assisted selective catalytic reduction (NH$_3$-SCR) in diesel exhaust systems. However, this catalyst is sensitive to small amounts of SO$_2$ in the exhaust gases, causing deactivation after prolonged exposure. To have a better understanding of the effect of the Si/Al ratio of zeolite on the SO$_2$ exposure of Cu-CHA catalysts, we measured *in situ* diffuse reflectance UV-vis NIR spectroscopy, SO$_2$ uptake, and deactivation of SO$_2$ poisoned Cu-CHA catalysts with the same Cu loading (3.2 wt%) and different Si/Al ratios (6.7, 11 and 15) at 200 °C. SO$_2$ selectively reacts with an oxygen-bridged diamine dicopper(II) complex [Cu$_2^{II}$(NH$_3$)$_4$O$_2$]$^{2+}$, resulting in 50% deactivation in all catalysts, with an SO$_2$ uptake which varies from a 0.2 S/Cu ratio for the catalyst with Si/Al = 6.7, to S/Cu = 0.12 for Si/Al = 15. For the fresh catalysts, the NH$_3$-SCR activity decreases as the Si/Al ratio increases from 6.7 to 15, as also indicated by the amount of [Cu$_2^{II}$(NH$_3$)$_4$O$_2$]$^{2+}$ complexes. After exposure of the [Cu$_2^{II}$(NH$_3$)$_4$O$_2$]$^{2+}$ complex to SO$_2$, the change in UV-vis spectra correlates well with the SO$_2$ uptake and the expected Cu-species formed for all three Si/Al ratios. This suggests that, under the applied conditions, the SO$_2$ reaction with the [Cu$_2^{II}$(NH$_3$)$_4$O$_2$]$^{2+}$ complex in Cu-CHA does not depend on the Si/Al ratio.

Introduction

Nitrogen oxides (NOx) are harmful by-products of diesel fuel combustion in automotive engines. The release of nitrogen oxides from diesel exhaust systems into the environment is regulated by various authorities, making it crucial to abate them before they are dispersed.[1] By employing the NH$_3$-SCR (selective catalytic reduction) reaction, NO$_X$ emissions from diesel exhaust systems can be effectively reduced. In the standard NH$_3$-SCR reaction, NO is reduced with NH$_3$ in the presence of O$_2$ to produce N$_2$ and H$_2$O with a stoichiometry of 4NO + 4NH$_3$ + O$_2$ → 4N$_2$ + 6H$_2$O.[2,3] Cu-Chabazite (CHA) small pore zeolites are commercialized catalysts for the NH$_3$-SCR reaction. Cu-CHA catalysts are highly active in the NH$_3$-SCR reaction, particularly at low temperatures, and demonstrate excellent thermal stability.[4,5]

The catalytic cycle for the NH$_3$-SCR reaction on the Cu-CHA catalyst at low temperatures (<250 °C) is based on an oxidation and a reduction part that involve Cu^I and Cu^{II} species with different ligands.[6,7] During the reduction part, the [Cu^I(NH$_3$)$_2$]$^+$ complex is an important intermediate with a certain mobility in the zeolite cage.[8] The oxidation step is crucial, as it involves the activation of O$_2$ by two [Cu^I(NH$_3$)$_2$]$^+$ complexes to form the [Cu$_2^{II}$(NH$_3$)$_4$O$_2$]$^{2+}$ complex.[9,10] The formation of [Cu$_2^{II}$(NH$_3$)$_4$O$_2$]$^{2+}$ is favored at high Cu density, with a fraction of unoxidized Cu^I that depends on the Cu loading and Si/Al ratio.[11,12] UV-vis spectroscopy can be used to monitor changes in the oxidation state of Cu during the formation of [Cu$_2^{II}$(NH$_3$)$_4$O$_2$]$^{2+}$, particularly in the d–d region (20 000–8000 cm^{-1} interval), where Cu^{II} ions in Cu-CHA have a specific fingerprint.[13–15] No absorption is observed in this region by Cu^I ions, since their d shell is filled.[16] Furthermore, the NIR (near-infrared) region of spectra allows for specific tracking of the ligands interacting with the Cu ions and the zeolite surface.[17]

The Cu-CHA catalyst is sensitive to SO$_2$ produced by the combustion of S-compounds in diesel fuel.[18–20] This causes a loss of activity below 350 °C, which is in the normal operation temperature range for NH$_3$-SCR catalysts.[21–23] Different studies have focused on the nature of the sulfur-based compounds formed during SO$_2$ exposure, which could be responsible for the deactivation. Namely, Cu bisulfite, Cu sulfate or bisulfate, ammonium sulfate or bisulfate, Al

[a] Umicore Denmark ApS, Kogle Allé 1, 2970 Hørsholm, Denmark.
E-mail: Ton.V.W.Janssens@eu.umicore.com
[b] Department of Chemistry and NIS Centre, University of Turin, Via Pietro Giuria 7, 10125 Turin, Italy. E-mail: gloria.berlier@unito.it

3076 | *Catal. Sci. Technol.*, 2024, **14**, 3076–3085

This journal is © The Royal Society of Chemistry 2024

sulfate, sulfuric acid and ammonium sulfate attached to Cu ions have been observed depending on the composition and treatments of catalysts.[21,22,24–29] These compounds are characterized by different thermal stabilities,[22,26,27,30] meaning that the activity of catalysts can be partially recovered by thermal treatments, typically above 350–400 °C.[19,22,27,29] X-ray absorption spectroscopy (XAS) measured during SO$_2$ exposure of Cu-CHA at low temperature after different pretreatments indicates that the $[Cu_2^{II}(NH_3)_4O_2]^{2+}$ complex is the most sensitive to SO$_2$. In contrast, Cu^I and Cu^{II} ions stabilized by the zeolite framework (fw-Cu^I and fw-Cu^{II}) are hardly affected by SO$_2$ exposure at 200 °C.[30] A two-step mechanism was proposed, where one SO$_2$ molecule reacts with two $[Cu_2^{II}(NH_3)_4O_2]^{2+}$ complexes, resulting in the formation of two $[Cu^I(NH_3)_2]^+$, one fw-Cu^I, and one Cu^{II}-sulfated compound.[31]

The Si/Al ratio of zeolite affects the formation of the $[Cu_2^{II}(NH_3)_4O_2]^{2+}$ complex,[11] which is an important intermediate in the NH$_3$-SCR reaction. A high Si/Al ratio resulted in a lower amount of $[Cu_2^{II}(NH_3)_4O_2]^{2+}$ complexes and a higher residual amount of $[Cu^I(NH_3)_2]^+$ after the oxidation part,[11] while catalysts with a low Si/Al ratio showed a higher yield of $[Cu_2^{II}(NH_3)_4O_2]^{2+}$ formation and higher catalytic activity.[32] These observations point to an influence of the Si/Al ratio on the NH$_3$-SCR reaction.[32]

In this study, the impact of SO$_2$ on the Cu-CHA catalyst in the NH$_3$-SCR reaction at 200 °C was investigated by employing *in situ* diffuse reflectance UV-vis-NIR spectroscopy, SO$_2$ uptake and deactivation measurements for three Cu-CHA catalysts with Si/Al ratios of 6.7, 11 and 15 and a Cu loading of 3.2 wt%. By examining the UV-vis spectra in the visible region (Cu^{II} d–d transitions) and the first-order rate constant measured at 200 °C, we investigated the effect of the Si/Al ratio on the formation of the $[Cu_2^{II}(NH_3)_4O_2]^{2+}$ complex and its reactivity to SO$_2$. We measured the deactivation and quantified the UV-vis absorption in the Cu^{II} d–d region to gain a better understanding of the impact of the Si/Al ratio on the SO$_2$ reaction with the $[Cu_2^{II}(NH_3)_4O_2]^{2+}$ complex.

Experimental

Three H-CHA (also known as H-SSZ-13) zeolites with Si/Al = 6.7, 11 and 15 were used to prepare Cu ion-exchanged chabazite zeolite catalysts by incipient wetness impregnation with the appropriate amount of an aqueous solution of Cu-nitrate to obtain a Cu loading of 3.2 wt%. The samples were impregnated by spraying the solution under stirring of the powder to obtain a more even distribution of Cu. Then, the samples were dried for 2 h at 90 °C, followed by 2 h of calcination at 600 °C in air to decompose the nitrates.

To determine the effect of SO$_2$ on the Cu-CHA catalysts, four well-defined Cu-species, namely framework-bound Cu^I and Cu^{II} (fw-Cu^I and fw-Cu^{II}) and $[Cu^I(NH_3)_2]^+$ and $[Cu_2^{II}(NH_3)_4O_2]^{2+}$ complexes, were prepared *in situ*, before exposure to SO$_2$ (see Fig. S1† for details). In short, fw-Cu^{II} is produced by oxidation in 10% O$_2$ at 400 °C,[17,30,33,34] fw-Cu^I is

produced by reduction of fw-Cu^{II} in 1% H$_2$ at 400 °C,[30] the $[Cu^I(NH_3)_2]^+$ complex is formed by exposure of the fw-Cu^{II} species to a mixture of 500 ppm NO and 600 ppm NH$_3$ at 200 °C,[12,35–37] and finally the $[Cu_2^{II}(NH_3)_4O_2]^{2+}$ complex is formed by exposure of $[Cu^I(NH_3)_2]^+$ to 10% O$_2$ at 200 °C.[11,12,30,37,38] The effect of exposure to 100 ppm SO$_2$ in N$_2$ on these four Cu-species was then determined by *in situ* diffuse reflectance (DR) UV-vis-NIR, SO$_2$ uptake and activity measurements.

For the DR UV-vis-NIR measurements, the spectra were recorded with a Varian Cary 5000 spectrophotometer, equipped with an R928 PMT UV-vis detector and a cooled PbS photocell NIR detector. The spectra were collected with a Praying Mantis® element, coupled with a low temperature reaction chamber, connected to a gas manifold system. For all UV-vis measurements, a 40 mg sample of the catalyst (sieve fraction 150–300 μm) was placed in the reaction chamber. Before each specific procedure described above and in Fig. S1,† the catalyst was first heated at 400 °C in 10% O$_2$ in N$_2$ with a total flow of 6 NL h^{-1} and left at this temperature for 1 hour, before cooling to the desired temperature. Teflon powder was used to measure the reference spectrum needed to determine the relative reflectance (R%):

$$R\% = \frac{R_{sample}}{R_{reference}} \times 100 \tag{1}$$

The Kubelka–Munk function was applied for semiquantitative comparison of the spectra in the region between 8000 and 20 000 cm^{-1}, characteristic of d–d transitions of Cu^{II} ions. The reflectance of the samples during the measurements was adjusted in the range of 20–50% in order to compare the calculated areas without artefacts due to a different vertical offset.[39]

The effect of SO$_2$ on the catalytic activity was determined using a powder flow reactor setup. The deactivation of the catalyst was determined as the ratio of the activities before and after exposure to 100 ppm SO$_2$ in N$_2$ at 200 °C. The entire procedure for the activity measurements is as follows: a sample of 10 mg of the fresh catalyst was diluted with 150 mg silicon carbide and added to a quartz U-tube reactor with an inner diameter of 4 mm; quartz wool was used to keep the catalysts as a fixed catalytic bed. The compositions of the feed and outlet gases were measured with a Gasmet CX4000 FTIR analyzer. First, the catalyst was subjected to heating at 550 °C in 10% O$_2$ in N$_2$ with a total flow of 12 NL h^{-1} and maintained at this temperature for 1 hour. To determine the activities, the catalyst was exposed to 500 ppm NO, 600 ppm NH$_3$, 10% O$_2$ and 5% H$_2$O (SCR gases) at 200 °C. Then, each Cu species was formed by the mentioned procedures and exposed to 100 ppm SO$_2$ in N$_2$. Subsequently, the catalyst was exposed to SCR gases to measure the activity of the SO$_2$ exposed catalyst. The activities were evaluated by determining the first-order rate constants, k (mol g$_{cat}^{-1}$ h^{-1}), for the fresh and SO$_2$ exposed catalysts with the following equations:

This journal is © The Royal Society of Chemistry 2024

Catal. Sci. Technol., 2024, **14**, 3076–3085 | **3077**

$$k = -\frac{F}{W} \ln(1-X) \qquad (2)$$

where F (mol h^{-1}) is the feed flow in the reactor, w (g$_{cat}$) is the mass of the catalyst and X is the conversion of NOx, *i.e.* NO + NO$_2$.

The ratio of the rate constants after and before the SO$_2$ exposure is then the measured for the deactivation:

$$\text{Deactivation (\%)} = \frac{k_{\text{deactivated}}}{k_{\text{Fresh}}} \times 100 \qquad (3)$$

The SO$_2$ uptake on the fw-Cu^I, fw-Cu^{II}, $[Cu^I(NH_3)_2]^+$, and $[Cu_2^{II}(NH_3)_4O_2]^{2+}$ complexes was measured in the same flow reactor setup and FTIR analyzer, using a 100 ppm SO$_2$/N$_2$ feed gas. After the preparation of the desired Cu species, the SO$_2$ concentration in the feed gas was measured for 15 min by bypassing the reactor, to obtain a good background. Then, the sample was exposed to 100 ppm SO$_2$/N$_2$ for 45 min at 200 °C, resulting in a lower SO$_2$ concentration at the outlet. After 45 min, the SO$_2$ concentration in the outlet reached the feed concentration again, indicating that the SO$_2$ uptake was complete (see Fig. 1). The SO$_2$ uptake was then calculated from integration of the SO$_2$ consumption curve (yellow area in Fig. 1) during the SO$_2$ exposure.

Results

Effect of SO$_2$ exposure on different Cu species

To determine the oxidation state of Cu for different Cu species, the d–d transitions in the 20 000–8000 cm^{-1} interval in the DR UV-vis spectra were investigated. The light coloured lines in Fig. 2 are the spectra obtained for the different Cu^I and Cu^{II} species in Cu-CHA with a Si/Al ratio of 6.7 before exposure to SO$_2$. The spectra for the Cu^{II} species show a clear absorption in the d–d transition region (panels a and d), while those for the Cu^I species do not (panels b and c). The $[Cu_2^{II}(NH_3)_4O_2]^{2+}$ complex exhibits an absorption in the d–d region, centered at 13 500 cm^{-1}, with slight variations in the position and shape compared to fw-Cu^{II} (Fig. 2a and d, respectively).[37] In summary, these spectra confirm the formation of well-defined Cu^{II} and Cu^I species, similar to what was observed by XAS after similar pre-treatments.[30]

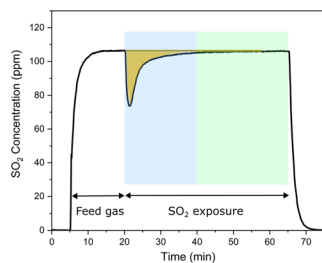The changes in the d–d transition upon SO$_2$ exposure reveal the different interactions of these four Cu species with
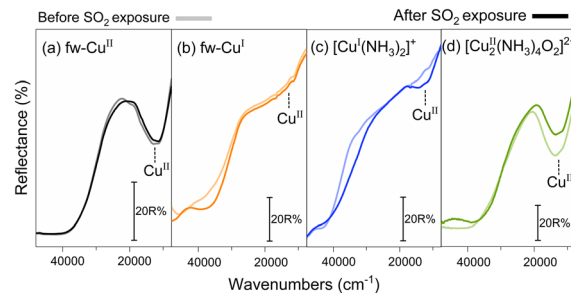

Fig. 2 Effect of SO$_2$ on different Cu species monitored by *in situ* DR UV-vis spectroscopy on Cu-CHA with a Si/Al ratio of 6.7 before (light lines) and after SO$_2$ exposure (dark lines) at 200 °C.

SO$_2$, (dark coloured lines in Fig. 2). For the $[Cu_2^{II}(NH_3)_4O_2]^{2+}$ complex, the fingerprint of Cu^{II} ions is affected, indicating an interaction of SO$_2$. The decrease in intensity indicates that some reduction of Cu has taken place, in good agreement with earlier results obtained by X-ray absorption spectroscopy.[30] On the other hand, the spectra for the framework-bound species are not affected by the exposure to SO$_2$. Notice that the spectra of fw-Cu^{II} and $[Cu_2^{II}(NH_3)_4O_2]^{2+}$ are hardly distinguishable in the d–d region, but their response to SO$_2$ is clearly different. The spectrum of the $[Cu^I(NH_3)_2]^+$ complex exhibits small changes, with a small portion of Cu^{II} being formed (Fig. 2c, dark coloured line). This change will be addressed in the Discussion section.

The interaction of NH$_3$ ligands on Cu species was investigated in the near-infrared (NIR) region (Fig. 3c and d). After exposing the sample to NO/NH$_3$ to obtain $[Cu^I(NH_3)_2]^+$ and $[Cu_2^{II}(NH_3)_4O_2]^{2+}$ complexes, the near-infrared (NIR) region shows the vibrational modes of NH$_3$ coordinated to Cu

Fig. 1 The SO$_2$ uptake of Cu-CHA with a Si/Al ratio of 6.7 during exposure to 100 ppm SO$_2$ in N$_2$ at 200 °C.
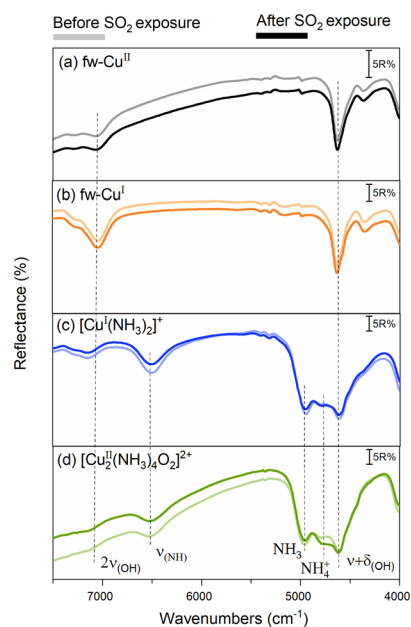

Fig. 3 Effect of SO$_2$ on different Cu species in the NIR region on sample Cu-CHA with a Si/Al ratio of 6.7 before (light lines) and after SO$_2$ exposure (dark lines) at 200 °C.

3078 | *Catal. Sci. Technol.*, 2024, **14**, 3076–3085

This journal is © The Royal Society of Chemistry 2024

Table 1 SO$_2$ uptakes and the corresponding S/Cu ratios for different Cu species after SO$_2$ exposure at 200 °C on Cu-CHA with a Si/Al ratio of 6.7

Cu state	fw-Cu^{II}	fw-Cu^{I}	$[Cu^{I}(NH_3)_2]^+$	$[Cu_2^{II}(NH_3)_4O_2]^{2+}$
SO$_2$ uptake (µmol SO$_2$ per g$_{Catalyst}$)	30	7	27	101
S/Cu ratio	0.02	0.06	0.05	0.2

ions and NH$_4^+$ formed by protonation from residual Brønsted sites.[40] More in detail, the band at 6510 cm^{-1} can be related to the overtone of the NH stretching modes of NH$_3$ and NH$_4^+$, with the corresponding stretching + bending combination modes at 4960 and 4730 cm^{-1}, respectively. These bands are absent in the NIR spectra of fw-Cu^{II} and fw-Cu^{I} (panels a and b, respectively) showing only the vibrational modes of silanols and Brønsted sites at 7050 and 4600 cm^{-1}.[17] After exposure to SO$_2$, all bands in the NIR region were unchanged, except for the NH$_4^+$ band, which shows a slight increase in the $[Cu_2^{II}(NH_3)_4O_2]^{2+}$ complex (Fig. 3d). This indicates that the presence of the $[Cu_2^{II}(NH_3)_4O_2]^{2+}$ complex leads to NH$_4^+$ formation after SO$_2$ exposure.

Having verified the higher sensitivity of the $[Cu_2^{II}(NH_3)_4O_2]^{2+}$ complex to SO$_2$, we have repeated the same protocols to measure the corresponding SO$_2$ uptakes and deactivation. The S/Cu ratio of the catalysts was determined by measuring SO$_2$ uptakes after each pretreatment. The SO$_2$ uptake for the $[Cu_2^{II}(NH_3)_4O_2]^{2+}$ complex is higher (S/Cu = 0.2), compared to those of the other Cu species, in agreement with the changes observed in the UV-vis spectra. The amount of SO$_2$ uptakes in µmol per gram of catalyst and the S/Cu ratio are in good agreement with what was reported in ref. 30 for the same catalyst (Table 1).

The NH$_3$-SCR activity of the same Cu-CHA catalyst was measured at 200 °C before and after SO$_2$ exposure in the four states described above. Fig. 4 reports the calculated deactivation (eqn (3)) as a function of SO$_2$ uptake, expressed as the S/Cu ratio. The data show that the deactivation increases linearly with the sulfur uptake. More in detail, the lowest deactivation (7%) corresponds to the catalyst
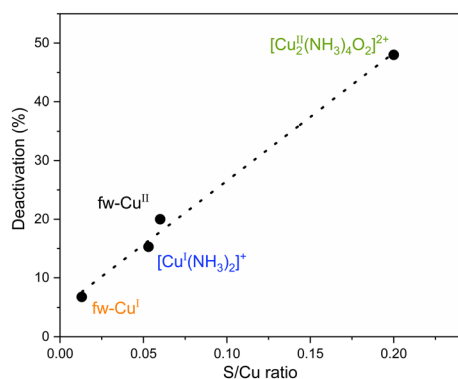

Fig. 4 Relationship between deactivation and SO$_2$ uptake for the four different Cu species in Cu-CHA with a Si/Al ratio of 6.7. SO$_2$ uptake was measured in 100 ppm SO$_2$ at 200 °C; deactivation was calculated by measuring NH$_3$-SCR activity in 500 ppm NO, 600 ppm NH$_3$, 10% O$_2$ and 5% H$_2$O at 200 °C, before and after SO$_2$ exposure.

pretreated to obtain fw-Cu^{I}, followed by $[Cu^{I}(NH_3)_2]^+$ (15%) and fw-Cu^{II} (20%). The catalyst measured after formation of the $[Cu_2^{II}(NH_3)_4O_2]^{2+}$ complex exhibits the highest SO$_2$ uptake and deactivation (50%) compared to the other species. This observation fits well with the measured UV-vis spectra, which indicates a significant reduction of Cu^{II} to Cu^{I} when SO$_2$ interacts with the $[Cu_2^{II}(NH_3)_4O_2]^{2+}$ complex. In summary, the catalyst exposing only fw-Cu^{I} sites can be exposed to SO$_2$ without loss of activity, while the activity decreases more when the Cu species are divalent and coordinated by NH$_3$ ligands.

Reducibility of the $[Cu_2^{II}(NH_3)_4O_2]^{2+}$ complex after SO$_2$ exposure followed by *in situ* DR UV-vis spectroscopy

The results discussed so far show that the Cu-CHA catalyst takes up more SO$_2$ after a pretreatment forming the $[Cu_2^{II}(NH_3)_4O_2]^{2+}$ complex, and this corresponds to the highest deactivation measured in this study. The deactivation is caused by a less efficient reduction of the $[Cu_2^{II}(NH_3)_4O_2]^{2+}$ complex by NO/NH$_3$ after SO$_2$ exposure. Because this reduction represents the reduction part of the NH$_3$-SCR cycle, a less effective reduction of the $[Cu_2^{II}(NH_3)_4O_2]^{2+}$ complex leads to a slower NH$_3$-SCR reaction.[6,33] The change in reducibility of the $[Cu_2^{II}(NH_3)_4O_2]^{2+}$ complex species by SO$_2$ was measured by exposing this species to 500 ppm NO/600 ppm NH$_3$ at 200 °C, without and with SO$_2$ exposure (see Fig. S2† for details about the procedure).

The complete $[Cu^{I}(NH_3)_2]^+$/$[Cu_2^{II}(NH_3)_4O_2]^{2+}$/$[Cu^{I}(NH_3)_2]^+$ redox cycle was followed by DR UV-vis spectroscopy on Cu-CHA with a Si/Al ratio of 6.7 (Fig. 5a). The data show that after the reaction with NO/NH$_3$, the $[Cu_2^{II}(NH_3)_4O_2]^{2+}$ complex is completely reduced to $[Cu^{I}(NH_3)_2]^+$ (red and blue spectra in Fig. 5a), in agreement with previous reports.[37] A reoxidation reproduced the original spectrum for the $[Cu_2^{II}(NH_3)_4O_2]^{2+}$ complex (green curve in Fig. 5a), indicating that all Cu can be reversibly reduced and oxidized. If the $[Cu_2^{II}(NH_3)_4O_2]^{2+}$ state is exposed to SO$_2$, some of the Cu is reduced (green and yellow curve in Fig. 5b), in agreement with previous XAS measurements and Fig. 2d.[30,31] The subsequent reduction with NO/NH$_3$ (red curve in Fig. 5b) does not restore the initial $[Cu^{I}(NH_3)_2]^+$ state, indicating that some of the Cu remains in a Cu^{II} state, and therefore, the Cu-CHA cannot be fully reduced to $[Cu^{I}(NH_3)_2]^+$ after exposure of $[Cu_2^{II}(NH_3)_4O_2]^{2+}$ to SO$_2$. This provides evidence for the less efficient reduction of Cu after exposure to SO$_2$; the reaction of SO$_2$ with the $[Cu_2^{II}(NH_3)_4O_2]^{2+}$ complex seems to remove a fraction of Cu^{II} sites from the redox Cu^{II}/Cu^{I} cycle.

(a) Without SO$_2$ exposure

1) First Reduction in NO/NH$_3$
2) Oxidation in 10% O$_2$
3) Second Reduction in NO/NH$_3$

(b) With SO$_2$ exposure

1) First Reduction in NO/NH$_3$
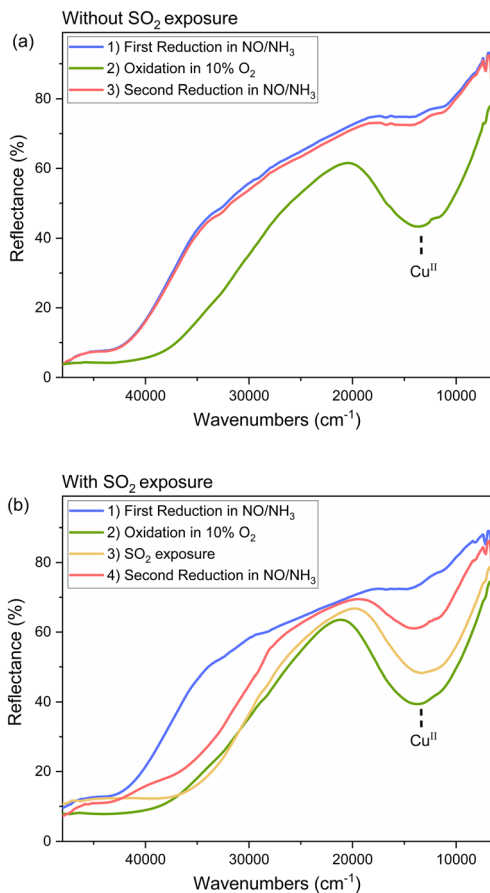2) Oxidation in 10% O$_2$
3) SO$_2$ exposure
4) Second Reduction in NO/NH$_3$

Fig. 5 a) Redox cycle of the $[Cu_2^{II}(NH_3)_4O_2]^{2+}$ complex in Cu-CHA with a Si/Al ratio of 6.7 followed by DR UV-vis: formation of $[Cu^I(NH_3)_2]^+$, reaction with O$_2$ to form the $[Cu_2^{II}(NH_3)_4O_2]^{2+}$ complex and subsequent reduction with NO/NH$_3$. b) as in a) with intermediate exposure of the $[Cu_2^{II}(NH_3)_4O_2]^{2+}$ complex to SO$_2$, followed by NO/NH$_3$. All spectra were measured at 200 °C.

Effect of the Si/Al ratio on the reactivity of the $[Cu_2^{II}(NH_3)_4O_2]^{2+}$ complex with SO$_2$

Having verified the higher reactivity of SO$_2$ with the $[Cu_2^{II}(NH_3)_4O_2]^{2+}$ complex with respect to the other Cu states in Cu-CHA with a Si/Al ratio of 6.7, we explored the same protocol as in Fig. 2d on other two Cu-CHA catalysts with the same Cu loading (3.2 wt%) and different Si/Al ratios (11 and 15). The UV-vis spectra measured before and after SO$_2$ interaction were converted into the Kubelka–Munk function, in order to make a semiquantitative comparison of the integrated area in the Cu^{II} d–d region.

Before SO$_2$ exposure (solid lines in Fig. 6a), the measured area should be proportional to the amount of the formed $[Cu_2^{II}(NH_3)_4O_2]^{2+}$ complex. It is clear from Fig. 6a and from the area values listed in Table 2 (1st column) that the band intensity follows the Si/Al order 6.7 > 11 > 15. This would imply an important effect of the catalyst Si/Al ratio (keeping constant the Cu loading) on the amount of the formed $[Cu_2^{II}(NH_3)_4O_2]^{2+}$ complex. Interestingly, the same trend is followed by the first order kinetic constant measured at 200
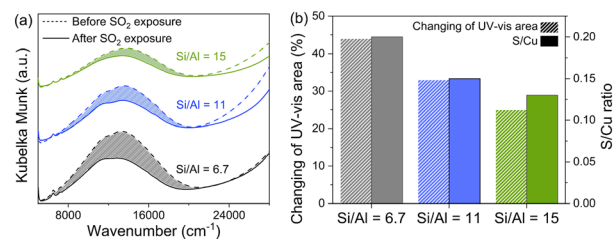

Fig. 6 a) Kubelka–Munk converted DR UV-vis spectra of Cu-CHA zeolite with different Si/Al ratios (6.7, 11 and 15) and the same loading (Cu = 3.2 wt%) in the d–d region; the spectra are vertically translated for clarity. b) Relative variation of the UV-vis area after SO$_2$ exposure and measured SO$_2$ uptake.

°C on the fresh catalysts (2nd column in Table 2) which is consistent with the hypothesis that the $[Cu_2^{II}(NH_3)_4O_2]^{2+}$ complex is relevant for the low temperature activity in the reaction (Fig. 7). In summary, a larger fraction of Cu is present as the $[Cu_2^{II}(NH_3)_4O_2]^{2+}$ complex at a low Si/Al ratio, and this is reflected in the measured kinetic constant.

All catalysts were exposed to SO$_2$ to compare changes of UV-vis area and measure SO$_2$ uptakes. As previously discussed, the exposure of the $[Cu_2^{II}(NH_3)_4O_2]^{2+}$ complex to SO$_2$ causes a decrease in the intensity of Cu^{II} d–d transitions (Fig. 6a, dashed lines). The relative variation in the spectral area (coloured area in Fig. 6) follows again the trend Si/Al 6.7 > 11 > 15. Thus, the catalyst showing the most abundant formation of the $[Cu_2^{II}(NH_3)_4O_2]^{2+}$ complex is the most affected by SO$_2$ exposure. This is also reflected in the SO$_2$ uptake measured under the same conditions (reported as the S/Cu ratio in Fig. 6b), which follows a similar trend.

Repeated SO$_2$ exposure and NH$_3$-SCR catalytic tests

Cu-CHA with a Si/Al ratio of 6.7 showed a deactivation of around 50% after SO$_2$ exposure of the $[Cu_2^{II}(NH_3)_4O_2]^{2+}$ complex. After the same procedure, the Cu-CHA samples with Si/Al ratios of 6.7, 11 and 15 show very similar deactivation values (50%, 57% and 53%, respectively) but different S/Cu ratios: 0.2, 0.15 and 0.13 for Cu-CHA with Si/Al ratios of 6.7, 11 and 15, respectively. To compare the SO$_2$ uptakes and deactivation for the three catalysts, we thus carried out experiments to take up more SO$_2$ and deactivate more catalysts. According to Fig. 1 (blue part), the catalysts' SO$_2$ uptake takes place in the first 20 min of SO$_2$ exposure. By repeating the cycle of reduction in NO/NH$_3$ followed by oxidation to form the $[Cu_2^{II}(NH_3)_4O_2]^{2+}$ complex and SO$_2$ exposure (see Fig. S3† for details about the procedure), the SO$_2$ uptake increases gradually, and the total amount is measured by adding the SO$_2$ uptake during each exposure step. The catalytic activity was measured after each SO$_2$ exposure to calculate the deactivation. Totally, these steps – reduction, oxidation, SO$_2$ exposure and measurement of catalytic activity – were repeated six times.

In Fig. 8, the deactivation measured at 200 °C is plotted as a function of the SO$_2$ uptakes, expressed as the S/Cu ratio. A

3080 | *Catal. Sci. Technol.*, 2024, **14**, 3076–3085

This journal is © The Royal Society of Chemistry 2024

Table 2 Initial UV-vis area of the $[Cu_2^{II}(NH_3)_4O_2]^{2+}$ complex and first-order rate constant at 200 °C for the different catalysts

Si/Al ratio	UV-vis area of the $[Cu_2^{II}(NH_3)_4O_2]^{2+}$ complex $\times 10^{-4}$ (cm^{-1})	Rate constant of fresh catalysts at 200 °C (mol NO per g_{cat} h^{-1})
6.7	0.58	80.1
11	0.43	51.9
15	0.315	37.6

good linearity is observed for each Si/Al ratio. As mentioned, all catalysts lose around 50% of their activity during the first cycle although the amount of SO$_2$ uptake is different. In the second cycle, the deactivation increases around 75%, meaning that a further 50% is lost with respect to the first poisoning cycle for all catalysts. This corresponds to an increase of the S/Cu ratio which is only half of the initial S/Cu ratio for the three catalysts. Both deactivation and the S/Cu ratio change by less than 50% in the following cycles, eventually reaching a stable level after several cycles. This
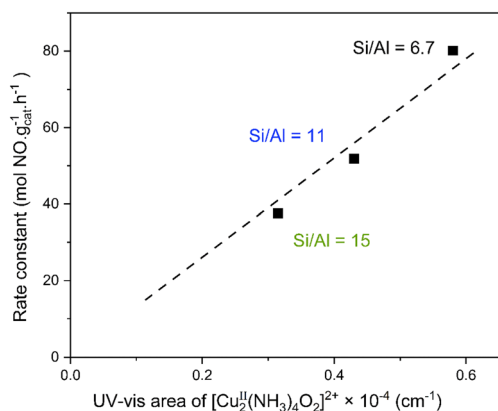
indicates that the deactivation behavior of the Cu-CHA catalysts through SO$_2$ exposure on the sensitive $[Cu_2^{II}(NH_3)_4-O_2]^{2+}$ complex is different from the beginning to the end, suggesting that complete deactivation of the catalyst is not achievable.

Discussion

SO$_2$ reaction with the $[Cu_2^{II}(NH_3)_4O_2]^{2+}$ complex causes Cu^{II}-sulfated formation and deactivation

DR UV-vis, SO$_2$ uptake and deactivation measurements confirm the sensitivity of the $[Cu_2^{II}(NH_3)_4O_2]^{2+}$ complex to SO$_2$ exposure. The $[Cu_2^{II}(NH_3)_4O_2]^{2+}$ complex is formed upon activation of O$_2$ by a pair of $[Cu^{I}(NH_3)]^+$ complexes, and therefore the reaction of SO$_2$ with $[Cu_2^{II}(NH_3)_4O_2]^{2+}$ is a key step in the deactivation mechanism. It has been proposed that the SO$_2$ poisoning is more pronounced upon exposure to a typical NH$_3$-SCR feed gas (NO/NH$_3$/O$_2$/H$_2$O mixture), as compared to an O$_2$/H$_2$O mixture.[41] This aligns well with the observation that SO$_2$ primarily interacts with the $[Cu_2^{II}(NH_3)_4O_2]^{2+}$ complex, because the formation of the $[Cu_2^{II}(NH_3)_4O_2]^{2+}$ complex requires the presence of both NO and NH$_3$, according to the NH$_3$-SCR reaction cycle.[6,7,37]

Moreover, we have shown by DR UV-vis that the catalyst cannot be completely reduced in NO/NH$_3$, closing the catalytic cycle, after the SO$_2$ reaction with the $[Cu_2^{II}(NH_3)_4-O_2]^{2+}$ complex. According to Molokova *et al.*, the SO$_2$ reaction with the $[Cu_2^{II}(NH_3)_4O_2]^{2+}$ complex causes the formation of a mixture of fw-Cu^I, $[Cu^{I}(NH_3)_2]^+$, a small amount of unreacted $[Cu_2^{II}(NH_3)_4O_2]^{2+}$ complex and a 'Cu^{II}-sulfated component', likely coordinated to NH$_3$ ligands.[28,30] This means that the band in the d–d region measured after SO$_2$ interaction is given by a fraction of the (active) $[Cu_2^{II}(NH_3)_4O_2]^{2+}$ complex and by this Cu^{II}-sulfated component, which does not react efficiently with NO/NH$_3$ to close the catalytic cycle and is thus responsible for the measured deactivation.

Notably, the observation of NH$_4^+$ formation in the NIR region only after SO$_2$ exposure of the $[Cu_2^{II}(NH_3)_4O_2]^{2+}$ complex could be related to the formation of some ammonium sulphate (NH$_4$)$_2$SO$_4$ or bisulfate (NH$_4$)HSO$_4$ as proposed by different authors.[22,25,42] However, the deactivation after the SO$_2$ reaction with the $[Cu_2^{II}(NH_3)_4O_2]^{2+}$ complex is not compatible with an accumulation of ammonium bisulfate causing the physical blocking on the zeolite pores. This mechanism is not compatible with the observation that a small amount of SO$_2$ (S/Cu = 0.2) causes a deactivation of 50%.

Fig. 7 Correlation between the first-order rate constant *versus* initial UV-vis area of the $[Cu_2^{II}(NH_3)_4O_2]^{2+}$ complex. The rate constant was calculated from catalytic activity measurements in 500 ppm NO, 600 ppm NH$_3$, 10% O$_2$ and 5% H$_2$O at 200 °C.
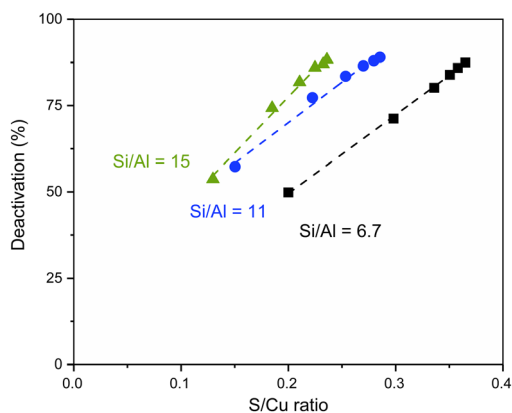

Fig. 8 The deactivation *versus* SO$_2$ uptake (S/Cu ratio) during repeated SO$_2$ exposure. NO conversion conditions: 500 ppm NO, 600 ppm NH$_3$, 10% O$_2$ and 5% H$_2$O at 200 °C. SO$_2$ exposure conditions: 100 ppm SO$_2$ at 200 °C, each point is related to one cycle.

This journal is © The Royal Society of Chemistry 2024

Catal. Sci. Technol., 2024, **14**, 3076–3085 | **3081**

Formation of the $[Cu_2^{II}(NH_3)_4O_2]^{2+}$ complex and SO_2 exposure on catalysts with different Si/Al ratios

The first-order rate constant at 200 °C for the three catalysts with identical Cu loading (3.2 wt%) exhibits a correlation with the obtained DR UV-vis spectra and the corresponding calculated Kubelka–Munk area. It is reasonable to consider that the UV-vis area in the Cu^{II} d–d region after the described experimental procedure is associated with the capability of the catalysts to form the $[Cu_2^{II}(NH_3)_4O_2]^{2+}$ complex. This implies a correlation between the rate constant and the amount of the formed $[Cu_2^{II}(NH_3)_4O_2]^{2+}$ complex, which can be monitored by DR UV-vis spectroscopy. This observation is in agreement with the hypothesis that the $[Cu_2^{II}(NH_3)_4O_2]^{2+}$ complex is the active site in the low temperature NH_3-SCR reaction, so that the kinetic constant depends on its concentration (Fig. 7). The concentration of the $[Cu_2^{II}(NH_3)_4O_2]^{2+}$ complex and the kinetic constant are higher for Cu-CHA with a Si/Al ratio of 6.7. We can hypothesize that this is due to the higher negative charge in the framework induced by the presence of Al, which would favour the divalent oxidation state. Thus, maintaining Cu as Cu^I species within the zeolite cages becomes more challenging.

After SO_2 exposure of the $[Cu_2^{II}(NH_3)_4O_2]^{2+}$ complex, all the catalysts showed a 50% decrease of activity after the first SO_2 exposure (Fig. 8), irrespective of the SO_2 uptake, which instead shows a linear correlation with the rate constant of the fresh catalysts (Fig. 9).

Following the deactivation mechanism by SO_2 on catalysts with different Si/Al ratios

Notably, a small S/Cu ratio (0.2 for Cu-CHA with a Si/Al ratio of 6.7) is capable of reducing the rate constant by 50%. Based on XAS data, coupled to the measurement of SO_2 uptake, Molokova *et al.* proposed a two-step mechanism where one single SO_2 molecule reacts with two $[Cu_2^{II}(NH_3)_4O_2]^{2+}$ complexes.[31] This, coupled to steric hindrance, could explain
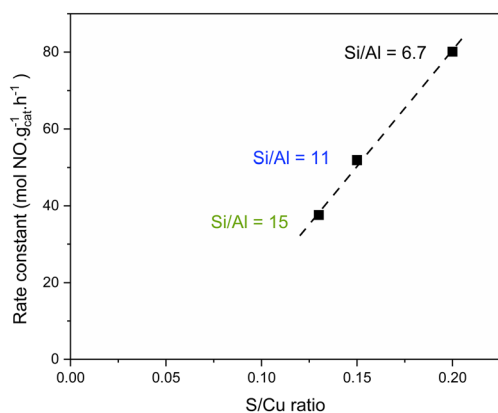

Fig. 9 Correlation between the first-order rate constant and SO_2 loading (S/Cu). The rate constant was calculated from catalytic activity measurements in 500 ppm NO, 600 ppm NH_3, 10% O_2 and 5% H_2O at 200 °C on the fresh catalysts.

the high impact on catalytic activity of a small SO_2 uptake.[42] The stoichiometry resulting from this mechanism is

$$2[Cu_2^{II}(NH_3)_4O_2]^{2+} + SO_2 \rightarrow 2Cu^I(NH_3)_2 + \text{fw-}Cu^I + Cu^{II}\text{-}SO_4Z \quad (4)$$
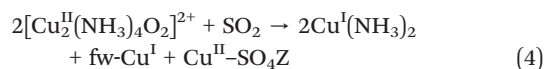
The sulfated species (Cu^{II}–SO_4Z) is characterized by a square-planar coordination of Cu with 4 ligands including oxygen and NH_3 as Z, as demonstrated by EXAFS and XANES analyses.[31] Based on this stoichiometry, we have considered as input for each catalyst the measured S/Cu ratio to calculate the fraction of formed Cu^{II}-sulfated and Cu^I species ($2Cu^I(NH_3)_2 + \text{fw-}Cu^I$), considering the rest of the Cu as unreacted $[Cu_2^{II}(NH_3)_4O_2]^{2+}$ (Table 3). For instance, an SO_2 uptake corresponding to S/Cu = 0.2 (Cu-CHA with a Si/Al ratio of 6.7, Table 3) would imply 20% Cu^{II}-sulfated components, 60% Cu^I species and 20% $[Cu_2^{II}(NH_3)_4O_2]^{2+}$ complexes. Thus, the UV-vis area in the d–d region measured in Cu-CHA with a Si/Al ratio of 6.7 (calibration sample) after SO_2 dosage would be due to 20% unreacted $[Cu_2^{II}(NH_3)_4O_2]^{2+}$ complexes plus 20% Cu^{II}-sulfated components. This assumption was used to estimate the relative absorption coefficient of Cu^{II}-sulfated components with respect to that of $[Cu_2^{II}(NH_3)_4O_2]^{2+}$. The obtained value (1.8) was then used to calculate the expected variation on Cu-CHA with Si/Al ratios of 11 and 15 based on the corresponding S/Cu ratios (second column of Table 3). The agreement between the calculated area variations and the measured ones (6th and 5th column of Table 3) is striking, supporting the validity of the mechanism proposed in ref. 31 for catalysts with three different Si/Al and S/Cu ratios.

The deactivation caused by SO_2 on the $[Cu_2^{II}(NH_3)_4O_2]^{2+}$ complex exhibits similar behavior across the catalysts with different Si/Al ratios, although the SO_2 uptakes are different. The rate constant measurements indicate a 50% decrease in activity when SO_2 reacts with the $[Cu_2^{II}(NH_3)_4O_2]^{2+}$ complex. It is interesting to notice that the activity of all catalysts further decreases by 50% in the second step of SO_2 exposure. This would suggest a mechanism where SO_2 affects half of the active $[Cu_2^{II}(NH_3)_4O_2]^{2+}$ complex in the first step, and half of the remaining $[Cu_2^{II}(NH_3)_4O_2]^{2+}$ complex in the second one. This does not happen in the following SO_2 exposure steps, which could be explained by the fact that the concentration of the $[Cu_2^{II}(NH_3)_4O_2]^{2+}$ complex is too small, and the accessibility to SO_2 is limited by the high concentration of the Cu^{II}-sulfated compound in the zeolite pores.

As a further comment, from the stoichiometry proposed in eqn (4), one SO_2 molecule would decompose two $[Cu_2^{II}(NH_3)_4O_2]^{2+}$ complexes, resulting in one inactive Cu^{II}-sulfated compound, two $[Cu^I(NH_3)_2]^+$ and one fw-Cu^I. This should result in a 25% decrease in activity for each SO_2, since the $[Cu^I(NH_3)_2]^+$ and fw-Cu^I sites should be still available for the NH_3-SCR reaction. Clearly, this is not in agreement with the deactivation measured in this work, suggesting that the poisoning mechanism is more complex.

3082 | *Catal. Sci. Technol.*, 2024, **14**, 3076–3085

This journal is © The Royal Society of Chemistry 2024

Table 3 Calculated percentage of Cu species formed in the three catalysts after SO_2 uptake based on the stoichiometry proposed in ref. 31 and measured S/Cu ratio, and the corresponding measured and calculated variations in UV-vis area

Si/Al ratio	Cu^{II} sulfated (S/Cu ratio)	$[Cu^I(NH_3)_2]^+$ and fw-Cu^I	$[Cu_2^{II}(NH_3)_4O_2]^{2+}$	UV-vis decrease (%)	
				Meas.	Calc.
6.7	**0.2**	0.60	0.20	**44**	—
11	**0.15**	0.45	0.40	33	33
15	**0.12**	0.36	0.52	25	26

Bold entries were measured values used as input for calculation of the UV-vis decrease in the d–d region after SO_2 uptake; Cu-CHA with a Si/Al ratio of 6.7 was used as a calibration sample.

O_2 sensitivity of Cu^I species on Cu-CHA catalysts

A small increase of Cu^I to Cu^{II} during SO_2 exposure of the $[Cu^I(NH_3)_2]^+$ complex was observed (Fig. 2c). However, the spectrum of fw-Cu^I does not change after SO_2 exposure, showing that SO_2 does not react with Cu^I. Moreover, SO_2 has been shown to reduce Cu^{II} to Cu^I, meaning that the observed oxidation of Cu^I to Cu^{II} for the $[Cu^I(NH_3)_2]^+$ complex cannot be related to the reaction with SO_2 itself, but could be related to the presence of small traces of oxygen stored in the sample. To explore this concept, the sensitivity of fw-Cu^I and $[Cu^I(NH_3)_2]^+$ species to O_2 was examined through pulse oxidation steps. Namely, the catalyst was exposed 10 times to

a 2% O_2/N_2 flow for 5 seconds after forming $[Cu^I(NH_3)_2]^+$ or fw-Cu^I species (Fig. 10a and b, respectively). Subsequently, the catalyst was left in O_2 for 30 min to achieve complete oxidation (see Fig. S4† for details about the measurement).

Fig. 10 illustrates the changes in the spectra after each O_2 pulse, leading to the formation of Cu^{II} species. It is evident that the mobile $[Cu^I(NH_3)_2]^+$ complex is more sensitive compared to the fw-Cu^I species. Indeed, the formation of the $[Cu_2^{II}(NH_3)_4O_2]^{2+}$ complex has been related to the ability of a couple of mobile $[Cu^I(NH_3)_2]^+$ complexes to activate O_2, while the oxidation of fw-Cu^I ions is more difficult.[43–45] Nevertheless, both Cu^I species can be oxidized to Cu^{II} in fully oxidizing environments at 200 °C. Notably, the rate of oxidation and the final spectral shape differ, indicating the formation of two different Cu^{II} species. These results indicate the high reactivity of $[Cu^I(NH_3)_2]^+$ to a small contamination or to the amount of oxygen stored in the catalysts in Cu_xO_y species.[30] Indeed, this suggests that the small amount of SO_2 uptake and deactivation after forming the $[Cu^I(NH_3)_2]^+$ complex could be related to the presence of a small amount of the $[Cu_2^{II}(NH_3)_4O_2]^{2+}$ complex.

Conclusions

In this study, we investigated the interaction of SO_2 with Cu-CHA catalysts with different Si/Al ratios at 200 °C, after specific pre-treatments to obtain well defined Cu^I and Cu^{II} species. DR UV-vis spectroscopy confirms the observation that SO_2 preferentially interacts with the $[Cu_2^{II}(NH_3)_4O_2]^{2+}$ complex, which is believed to be an important intermediate in the NH$_3$-SCR reaction at low temperature.

This interaction results in a reduction of Cu^{II} to Cu^I and in the formation of a Cu^{II}-sulfated compound, which cannot be reduced by NO/NH$_3$. This indicates that the Cu^{II}-sulfated compound is responsible for the observed loss of activity.

The Si/Al ratio of the zeolite affects the amount of the formed $[Cu_2^{II}(NH_3)_4O_2]^{2+}$ complex, as measured by UV-vis spectroscopy, showing a correlation with the reaction rate measured at 200 °C, which is in the order 6.7 > 11 > 15. The same trend is observed for the SO_2 uptake measured after SO_2 interaction with the $[Cu_2^{II}(NH_3)_4O_2]^{2+}$ complex. However, the three catalysts show similar deactivation of around 50% after the first SO_2 exposure. Repeated SO_2 exposure cycles show a correlation between SO_2 accumulation and
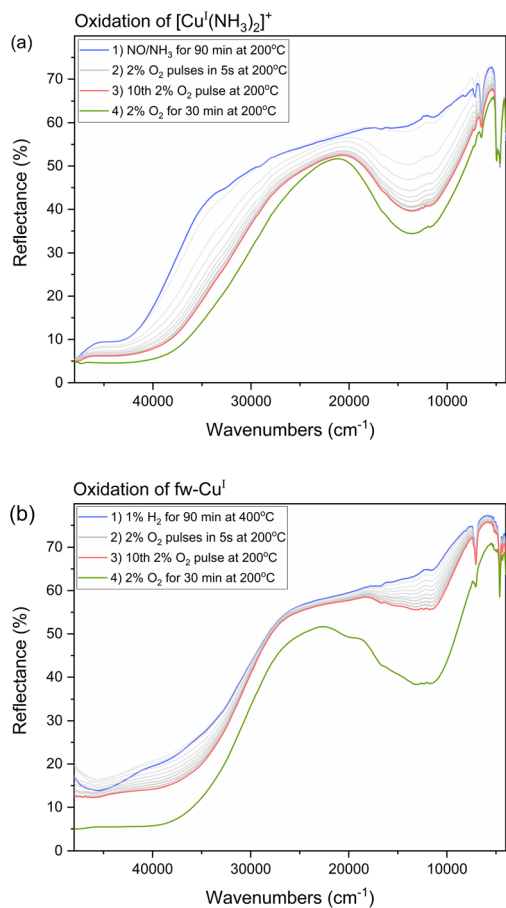

Fig. 10 DR UV-vis experiments: 5 s 2% O_2 pulses on a) $[Cu^I(NH_3)_2]^+$ and b) fw-Cu^I on Cu-CHA with a Si/Al ratio of 6.7 at 200 °C.

This journal is © The Royal Society of Chemistry 2024

Catal. Sci. Technol., 2024, **14**, 3076–3085 | **3083**

deactivation for the three catalysts, with both parameters gradually levelling off.

The measured changes in the UV-vis after SO_2 interaction with the $[Cu_2^{II}(NH_3)_4O_2]^{2+}$ complex is consistent with the formation of the Cu^{II}-sulfated compound following a reaction mechanism recently proposed.[31] This in turns indicates that the same reaction mechanism takes place in the three catalysts, irrespective of the Si/Al ratio.

Author contributions

Reza K. Abasabadi: measurements, data analysis, interpretation, and writing. Ton V. W. Janssens and Gloria Berlier: conceptualization, interpretation, editing, supervision, and funding. Silvia Bordiga: interpretation.

Conflicts of interest

There are no conflicts to declare.

Acknowledgements

References

1 A. Wang and L. Olsson, *Nat. Catal.*, 2019, **2**, 566–570.
2 R. Gounder and A. Moini, *React. Chem. Eng.*, 2019, **4**, 966–968.
3 I. Nova and E. Tronconi, *Urea-SCR technology for deNOx after treatment of diesel exhausts*, 2014, vol. 5.
4 C. H. F. Peden, *J. Catal.*, 2019, **373**, 384–389.
5 E. Borfecchia, K. A. Lomachenko, F. Giordanino, H. Falsig, P. Beato, A. V. Soldatov, S. Bordiga and C. Lamberti, *Chem. Sci.*, 2015, **6**, 548–563.
6 Y. Feng, X. Wang, T. V. W. Janssens, P. N. R. Vennestrøm, J. Jansson, M. Skoglundh and H. Grönbeck, *ACS Catal.*, 2021, **11**, 14395–14407.
7 L. Chen, T. V. W. Janssens, P. N. R. Vennestrøm, J. Jansson, M. Skoglundh and H. Grönbeck, *ACS Catal.*, 2020, **10**, 5646–5656.
8 R. Millan, P. Cnudde, V. Van Speybroeck and M. Boronat, *JACS Au*, 2021, **1**, 1778–1787.
9 X. Wang, L. Chen, P. N. R. Vennestrøm, T. V. W. Janssens, J. Jansson, H. Grönbeck and M. Skoglundh, *ChemCatChem*, 2021, **13**, 2577–2582.
10 F. Gao, D. Mei, Y. Wang, J. Szanyi and C. H. F. Peden, *J. Am. Chem. Soc.*, 2017, **139**, 4935–4942.
11 A. Martini, C. Negri, L. Bugarin, G. Deplano, R. K. Abasabadi, K. A. Lomachenko, T. V. W. Janssens, S. Bordiga, G. Berlier and E. Borfecchia, *J. Phys. Chem. Lett.*, 2022, **13**, 6164–6170.
12 C. Paolucci, I. Khurana, A. A. Parekh, S. Li, A. J. Shih, H. Li, J. R. Di Iorio, J. D. Albarracin-Caballero, A. Yezerets, J. T. Miller, W. N. Delgass, F. H. Ribeiro, W. F. Schneider and R. Gounder, *Science*, 2017, **357**, 898–903.
13 F. Giordanino, P. N. R. Vennestrøm, L. F. Lundegaard, F. N. Stappen, S. Mossin, P. Beato, S. Bordiga and C. Lamberti, *Dalton Trans.*, 2013, **42**, 12741–12761.
14 H. Li, C. Paolucci, I. Khurana, L. N. Wilcox, F. Göltl, J. D. Albarracin-Caballero, A. J. Shih, F. H. Ribeiro, R. Gounder and W. F. Schneider, *Chem. Sci.*, 2019, **10**, 2373–2384.
15 C. Tyrsted, E. Borfecchia, G. Berlier, K. A. Lomachenko, C. Lamberti, S. Bordiga, P. N. R. Vennestrøm, T. V. W. Janssens, H. Falsig, P. Beato and A. Puig-Molina, *Catal. Sci. Technol.*, 2016, **6**, 8314–8324.
16 B. Centrella, G. Deplano, A. Damin, M. Signorile, M. Tortora, C. Barolo, M. Bonomo and S. Bordiga, *Dalton Trans.*, 2022, **51**, 14439–14451.
17 C. Negri, M. Signorile, N. G. Porcaro, E. Borfecchia, G. Berlier, T. V. W. Janssens and S. Bordiga, *Appl. Catal., A*, 2019, **578**, 1–9.
18 P. S. Hammershøi, A. D. Jensen and T. V. W. Janssens, *Appl. Catal., B*, 2018, **238**, 104–110.
19 P. S. Hammershøi, Y. Jangjou, W. S. Epling, A. D. Jensen and T. V. W. Janssens, *Appl. Catal., B*, 2018, **226**, 38–45.
20 L. Ge, A. Wang, X. Hu, J. Zhang, J. He, P. Wang, L. Han and D. Zhang, *Catal. Sci. Technol.*, 2023, **13**, 4186–4196.
21 V. V. Mesilov, S. L. Bergman, S. Dahlin, Y. Xiao, S. Xi, M. Zhirui, L. Xu, W. Chen, L. J. Pettersson and S. L. Bernasek, *Appl. Catal., B*, 2021, **284**, 119756.
22 J. Du, X. Shi, Y. Shan, G. Xu, Y. Sun, Y. Wang, Y. Yu, W. Shan and H. He, *Catal. Sci. Technol.*, 2020, **10**, 1256–1263.
23 J. Ma, S. Chang, F. Yu, H. Lai and Y. Zhao, *Catalysts*, 2022, **12**, 1499–1510.
24 Y. Qiu, C. Fan, C. Sun, H. Zhu, W. Yi, J. Chen, L. Guo, X. Niu, J. Chen, Y. Peng, T. Zhang and J. Li, *Catalysts*, 2020, **10**, 1–12.
25 K. Wijayanti, K. Leistner, S. Chand, A. Kumar, K. Kamasamudram, N. W. Currier, A. Yezerets and L. Olsson, *Catal. Sci. Technol.*, 2016, **6**, 2565–2579.
26 Y. Jangjou, D. Wang, A. Kumar, J. Li and W. S. Epling, *ACS Catal.*, 2016, **6**, 6612–6622.
27 Y. Jangjou, Q. Do, Y. Gu, L. G. Lim, H. Sun, D. Wang, A. Kumar, J. Li, L. C. Grabow and W. S. Epling, *ACS Catal.*, 2018, **8**, 1325–1337.
28 S. L. Bergman, S. Dahlin, V. V. Mesilov, Y. Xiao, J. Englund, S. Xi, C. Tang, M. Skoglundh, L. J. Pettersson and S. L. Bernasek, *Appl. Catal., B*, 2020, **269**, 118722.
29 V. Mesilov, S. Dahlin, S. L. Bergman, S. Xi, J. Han, L. Olsson, L. J. Pettersson and S. L. Bernasek, *Appl. Catal., B*, 2021, **299**, 120626–120638.
30 A. Yu. Molokova, E. Borfecchia, A. Martini, I. A. Pankin, C. Atzori, O. Mathon, S. Bordiga, F. Wen, P. N. R. Vennestrøm, G. Berlier, T. V. W. Janssens and K. A. Lomachenko, *JACS Au*, 2022, **2**, 787–792.
31 A. Yu. Molokova, R. K. Abasabadi, E. Borfecchia, O. Mathon, S. Bordiga, F. Wen, G. Berlier, T. V. W. Janssens and K. A. Lomachenko, *Chem. Sci.*, 2023, **14**, 11521–11531.
32 S. H. Krishna, A. Goswami, Y. Wang, C. B. Jones, D. P. Dean, J. T. Miller, W. F. Schneider and R. Gounder, *Nat. Catal.*, 2023, **6**, 276–285.

3084 | *Catal. Sci. Technol.*, 2024, **14**, 3076–3085

This journal is © The Royal Society of Chemistry 2024

33 C. Negri, A. Martini, G. Deplano, K. A. Lomachenko, T. V. W. Janssens, E. Borfecchia, G. Berlier and S. Bordiga, *Phys. Chem. Chem. Phys.*, 2021, **23**, 18322–18337.

34 E. Borfecchia, K. A. Lomachenko, F. Giordanino, H. Falsig, P. Beato, A. V. Soldatov, S. Bordiga and C. Lamberti, *Chem. Sci.*, 2015, **6**, 548–563.

35 T. V. W. Janssens, H. Falsig, L. F. Lundegaard, P. N. R. Vennestrøm, S. B. Rasmussen, P. G. Moses, F. Giordanino, E. Borfecchia, K. A. Lomachenko, C. Lamberti, S. Bordiga, A. Godiksen, S. Mossin and P. Beato, *ACS Catal.*, 2015, **5**, 2832–2845.

36 K. A. Lomachenko, E. Borfecchia, C. Negri, G. Berlier, C. Lamberti, P. Beato, H. Falsig and S. Bordiga, *J. Am. Chem. Soc.*, 2016, **138**, 12025–12028.

37 C. Negri, T. Selleri, E. Borfecchia, A. Martini, K. A. Lomachenko, T. V. W. Janssens, M. Cutini, S. Bordiga and G. Berlier, *J. Am. Chem. Soc.*, 2020, **142**, 15884–15896.

38 A. Oda, H. Shionoya, Y. Hotta, T. Takewaki, K. Sawabe and A. Satsuma, *ACS Catal.*, 2020, **10**, 12333–12339.

39 F. C. Meunier, *React. Chem. Eng.*, 2016, **1**, 134–141.

40 F. Giordanino, E. Borfecchia, K. A. Lomachenko, A. Lazzarini, G. Agostini, E. Gallo, A. V. Soldatov, P. Beato, S. Bordiga and C. Lamberti, *J. Phys. Chem. Lett.*, 2014, **5**, 1552–1559.

41 K. Wijayanti, K. Xie, A. Kumar, K. Kamasamudram and L. Olsson, *Appl. Catal., B*, 2017, **219**, 142–154.

42 J. D. Bjerregaard, M. Votsmeier and H. Grönbeck, *J. Catal.*, 2023, **417**, 497–506.

43 H. Falsig, P. N. R. Vennestrøm, P. G. Moses and T. V. W. Janssens, *Top. Catal.*, 2016, **59**, 861–865.

44 L. Chen, H. Falsig, T. V. W. Janssens, J. Jansson, M. Skoglundh and H. Grönbeck, *Catal. Sci. Technol.*, 2018, **8**, 2131–2136.

45 L. Chen, H. Falsig, T. V. W. Janssens and H. Grönbeck, *J. Catal.*, 2018, **358**, 179–186.

This journal is © The Royal Society of Chemistry 2024

Catal. Sci. Technol., 2024, **14**, 3076–3085 | **3085**